JOURNAL OF CATALYSIS **161,** 409–422 (1996)
ARTICLE NO. 0199

Methane Reforming Reaction with Carbon Dioxide Over Ni/SiO_2 Catalyst

I. Deactivation Studies

V. C. H. Kroll, H. M. Swaan, and C. Mirodatos[1]

Institut de Recherches sur la Catalyse, CNRS, 2 Avenue Albert Einstein, F-69626 Villeurbanne Cédex, France

Received November 3, 1995; revised February 14, 1996; accepted February 29, 1996

The deactivation of Ni/SiO_2 catalysts under the conditions of carbon dioxide reforming of methane was studied as a function of different operating parameters. Several techniques have been used: temperature programmed hydrogenation, magnetic measurements, transmission electron microscopy, and thermogravimetric analysis. It was shown that, whatever the pretreatment, nickel carbide constituted the active phase for this reaction, being established in the very initial period of operation. The reaction mixture was found to be able to reduce the nickel phase on stream. The two major aging factors, namely nickel sintering and carbon deposition, were shown to be strongly related to the pretreatment conditions. A model is proposed to explain the influence of the analyzed operating parameters on the nature of the coke formation and on the changes in morphology of the nickel particles. Optimal operating conditions for the above catalyst for CO_2 reforming are defined.

INTRODUCTION

The reaction of methane reforming by carbon dioxide as a source of carbon monoxide and hydrogen is a major issue in heterogeneous catalysis (1). Noble metals perform as catalysts for this reaction (2–4). However, economic constraints have stimulated research on cheaper metals such as ferrous metals (Fe, Co, and Ni) which have been reported as a worthwhile alternative to noble metals, as recently reviewed by Tsang *et al.* (5). Disadvantages such as deactivation by particle sintering and/or by reaction with the support have been reported for nickel-based catalysts at temperatures around 800°C (2). At lower temperatures (600–700°C) carbon deposition was also considered as an aging factor for nickel-based catalysts. Several types of carbon were detected by Sacco *et al.* (6) and Jablonski *et al.* (7), who investigated the formation of carbon over nickel foils at 700°C. However, the origin of the carbon was not investigated directly, but only on the basis of kinetic measurements. It was concluded that methane could be the source of carbon (6). However, as stressed by Nolan *et al.* (8), the formation of carbon is accelerated in the presence of hydrogen. Rostrup-Nielsen and Bak Hansen (3) have suggested that the coke deposition can be avoided by sulfur passivation.

Preliminary temperature programmed oxidation (TPO) experiments carried out in our laboratory (9) revealed that at least two types of carbon were formed during the reforming reaction at 700°C over nickel-on-silica catalysts. One type, appearing very rapidly after contacting the catalyst with the reacting mixture, was easily oxidized at 500°C. A second type of carbon, accumulating during time-on-stream, was oxidized only around 700°C. In continuation of this work on nickel-based catalysts, the different routes of carbon formation and the eventual sintering processes in connection with the main pathways of the overall reaction mechanism have been investigated over a Ni/SiO_2 catalyst. Part I of this study aims at understanding the actual causes of catalyst aging during methane reforming with carbon dioxide. The origin and nature of carbon deposits have been studied by means of temperature programmed hydrogenation (TPH) and transmission electron microscopy (TEM). The morphological changes in the nickel particles have been followed by magnetic measurements. Part II will focus on the main mechanistic routes of the proper reforming reaction, investigated by steady-state isotopic transient kinetic analysis (SSTIKA) and *in situ* diffuse reflectance infrared Fourier transform (DRIFT) spectroscopy.

EXPERIMENTAL

Catalyst preparation and pretreatment. The nickel-on-silica catalyst was prepared by wet impregnation of a Degussa Aerosil P200 support with a $Ni(NH_3)_6NO_3$ solution, as already described in Ref. (10). After evaporation, the precursor was dried at 120°C. Calcination of the catalyst samples was performed *ex situ* under flowing oxygen at 750°C for 8 h. The nickel content was determined to be 4.0 wt%. Reduction was carried out *in situ* at 750°C for 10 h under flowing hydrogen (flowrate 1.2 liters/h, temperature

[1] To whom correspondence should be addressed.

0021-9517/96 $18.00

rise rate 2.5°C/min). The size of the catalyst pellets used for reaction was in the range of 0.2–0.3 mm.

Catalyst aging during methane reforming by CO_2. The steady-state activity of the catalysts was measured at 600 and 700°C at atmospheric pressure with a reaction mixture consisting of 15 vol% methane, 15 vol% carbon dioxide, and argon as diluent with a total flow rate of 7.2 liters/h. Typically 100 mg of catalyst was loaded either in a quartz microreactor, or in a special quartz cell allowing both catalytic and magnetic measurements without catalyst transfer in the open air (10). The external thermocouple was located at the same level as the catalyst bed. The microreactor had an internal diameter of 4 mm; the length of the catalyst bed was approximately 15 mm. In case of the special cell the length of the bed was approximately 6 mm, while the internal diameter was 6 mm. The product stream was analyzed by gas chromatography (HP 5890 Series II equipped with a Carboxen column) using a TCD for the detection of the reaction products.

Catalyst characterization. TPH experiments were carried out over aged catalysts by cooling them under helium and then raising the temperature from 25 to 1000°C at 20°C/min under a mixture H_2/He = 30/70, with a flowrate of 4.2 liters/h. Gases were analyzed by on-line mass spectrometry (VG Pegasus). The desorption peaks, corrected for fragmentation and background, were decomposed and integrated. Several peak shapes and types of peaks (e.g., symmetric, asymmetric, Gaussian and Lorentzian) were tested without showing major influence on the calculation of the decomposed peak areas. The corresponding amounts were determined after proper calibration of the mass spectrometer.

The degree of ferromagnetic nickel (i.e., the fraction of ferromagnetic nickel) and dispersion were determined at various stages of the reaction by means of magnetic measurements carried out in the special cell mentioned above and using the Weiss extraction method (11).

The following gases were used: methane (Alpha Gaz, purity >99.995%), carbon dioxide (Alpha Gaz, purity >99.995%), argon (Air Liquide, purity >99.995%), and helium (Carboxyque France, purity >99.998%).

Complementary experiments of thermogravimetric analysis (TGA) were carried out in a thermobalance unit (C. I. Electronics). Weight data were automatically collected every 30 s with an accuracy of ±0.001 mg and sent to a personal computer for storage and analysis. In all experiments 202 mg of catalyst and a flowrate of 14.4 liters/h were used at 700 or 600°C, the reactor being preheated under helium. The sample was held in a stainless steel gauze basket with a sieve opening of 125 μm. The gas mixture consisted of $CH_4 : CO_2 : N_2$ (15 : 15 : 70). For experiments at 700°C precalcined samples were used that were subsequently reduced or not. At 600°C noncalcined samples were used with or without a subsequent reduction step.

TEM investigations were performed on a JEOL JEM 2010 instrument with a maximum resolution of 3 Å. The samples were partly dissolved in ethanol and deposited on a copper grid.

RESULTS

Influence of pretreatment conditions on catalyst deactivation. Figure 1 reports the deactivation curves (CH_4 conversion vs time-on-stream) observed in the combined reaction/magnetic characterization cell as a function of the following pretreatment conditions: no pretreatment (dried at 120°C, but neither calcined nor reduced), calcination (dried at 120°C and calcined at 750°C, no reduction), or reduction (dried at 120°C and reduced at 750°C, no calcination). Table 1 reports the average aging rates, together with the corresponding catalyst characteristics obtained by magnetic measurements before and after reaction.

The maximum possible conversions corresponding to thermodynamic equilibrium have been calculated. The following reactions were taken into account: the CO_2 reforming reaction, the water gas shift reaction, and the Boudouard coking reaction (2). However, the major problem with these calculations consists in the data used for the carbon deposited on the catalyst surface. Generally, graphitic carbon is chosen but it has been shown in the literature that, depending on the type of carbon deposited or taking part in the reaction, the equilibrium may vary (12, 13). The calculations showed that under our conditions the maximum conversions were, for CH_4, 86 and 93%, and, for CO_2, 43 and 69%, at 600 and 700°C, respectively. If one

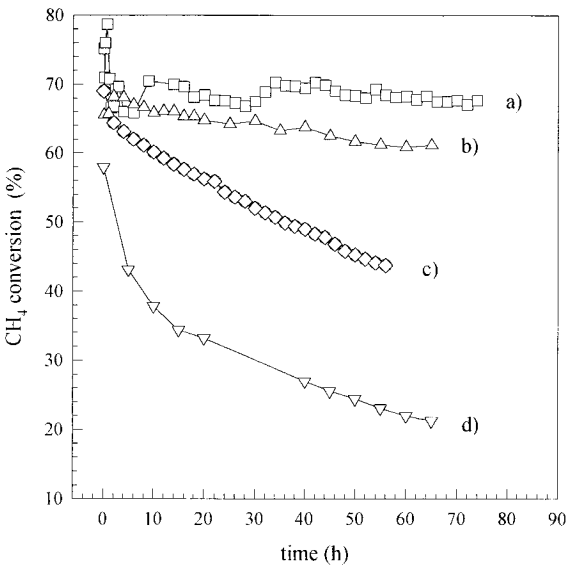

FIG. 1. Deactivation profiles of Ni/SiO_2 at 700°C with different pretreatments: (a) without any pretreatment, (b) calcined, (c) reduced at 750°C, (d) reduced at 900°C.

TABLE 1

Aging Data and Characteristics of Ni/SiO_2 before and after Catalytic Test at 700°C, as a Function of Pretreatment Conditions

Pretreatment	Time-on-stream (h)	Particle size (Å)		Dispersion (%)		Degree of reduction (%)		Methane conversion (%)		Average deactivation rate (% h^{-1})
		Before reaction	After reaction	Before reaction	After reaction	Before reaction	After reaction	Initial	Final	
None	75	—	77	—	15	0	92	75.2	67.7	0.10
Calcined	67	—	81	—	14	0	96	65.6	61.2	0.07
Red./750°C	65	63	78	17	14	62	71	69.0	43.8	0.39
Red./900°C	65	135	≈150[a]	9	7	99	84	58.0	21.3	0.55
Calcined[b]	240	—	—	—	—	—	—	76.0	72.7	0.01

[a] When particles larger than about 150 Å were present in the size distribution; i.e., when the samples could not be considered as superparamagnetic (as revealed by the presence of remanent magnetization) the determination of a precise average particle size was no more possible (11). Only an approximate value was considered for this case.

[b] Data obtained in a microreactor without magnetic measurements.

assumed that the Boudouard coking reaction was not taking place a completely different situation was observed. The maximum conversions were, for CH_4, 46 and 77%, and, for CO_2, 59 and 85%, at 600 and 700°C, respectively. This shows the importance of the data used for the carbon included in the model and the lack of reliability of these calculations.

It can be seen (Fig. 1) that whatever the pretreatment, most of the catalysts exhibited similar initial activities, measured after 5 min on stream. Note that the around two-times lower activity measured for the badly dispersed sample reduced at 900°C (curve d) corresponded roughly to the around two-times lower Ni dispersion (Table 1). Thereafter the catalysts tended to deactivate nonlinearly in the first period of the run, before the rate of deactivation reached almost constant values. These values appeared to highly dependent on the pretreatment conditions, as shown in Table 1. Thus the catalysts which were reduced before reaction lost their activity more rapidly (0.39 and 0.55% h^{-1} for samples reduced at 750 and 900°C, respectively). In contrast, the catalysts that did not undergo any pretreatment or that were only calcined showed a markedly enhanced stability (aging rate of 0.10 and 0.07% h^{-1}, respectively).

In order to check the influence of the type of reactor used for the aging study, a long-term run was performed in a microreactor with the Ni/SiO_2 catalyst that only underwent a calcination. A remarkable stability was observed, since after 250 h this catalyst lost only 3% of its initial activity (aging rate of 0.01% h^{-1}, Table 1, bottom line). A rather low but still significant amount of coke deposits was determined by TPO carried out after the run in the microreactor (12 mg_{coke}/g_{cat}) as compared with the coke deposits measured in the combined magnetic cell (e.g., 25 mg_{coke}/g_{cat} after 67 h) under similar operating conditions. The improved catalytic stability in the microreactor was probably related to better characteristics with respect to radial temperature profiles. The combined reaction/magnetic cell presented an internal diameter 1.5 times larger than the microreactor.

To summarize, besides some reactor configuration effects a detrimental effect of the catalyst prereduction on the catalytic stability was clearly observed.

Catalyst evolution during reaction. From Table 1, it can be noted that:

(i) After reaction, a high degree of ferromagnetic nickel (92–96%) was observed for nonpretreated or precalcined samples, while the prereduced samples displayed a significantly lower content of ferromagnetic nickel (71 and 84% for the samples reduced at 750 and 900°C, respectively). Chemical analysis performed on aged samples did not detect any loss of nickel phase, whatever the pretreatment.

(ii) The mean Ni particle size increased slightly for the prereduced samples, for which the initial dispersion was indeed available for comparison. This sintering effect was even more pronounced for the initially badly dispersed sample (reduced at 900°C), for which particles larger than 150 Å developed, as attested by the appearance of remanent magnetization (10, 11). For the case of untreated or calcined samples, the nickel dispersion observed on the aged samples was close to the one observed on the sample reduced at 750°C. No significant change in BET surface area was noted, attesting the stability of the silica surface during time-on-stream.

In order to follow the continuous changes of nickel state and morphology with time-on-stream, combined magnetic measurements and catalytic reaction were carried out on an untreated sample, i.e., for the case of optimized catalytic stability. A fresh catalyst precursor was thus exposed to the reacting mixture at 700°C. After 5 min the reactor was flushed with helium to remove the adsorbed species present on the catalyst surface, and cooled down to room temperature. A magnetic measurement was performed giving the degree of ferromagnetic nickel and its dispersion. Then the reactor was placed again in the oven at 700°C and the reacting

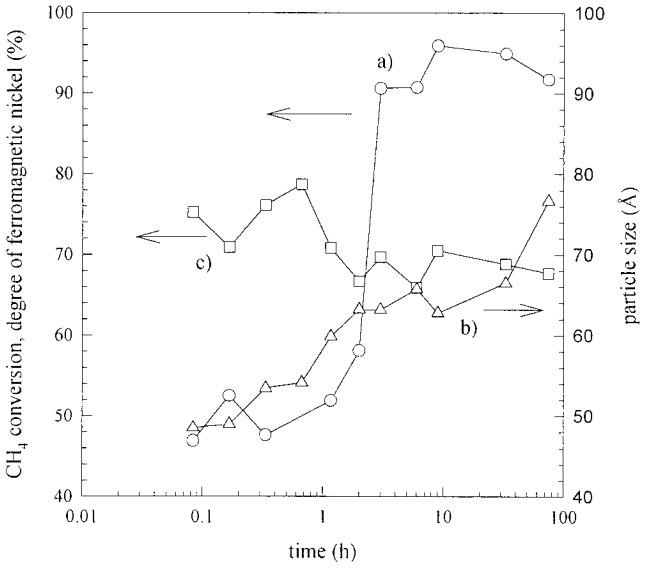

FIG. 2. (a) The degree of ferromagnetic nickel, (b) the particle size, and (c) the methane conversion as a function of time-on-stream.

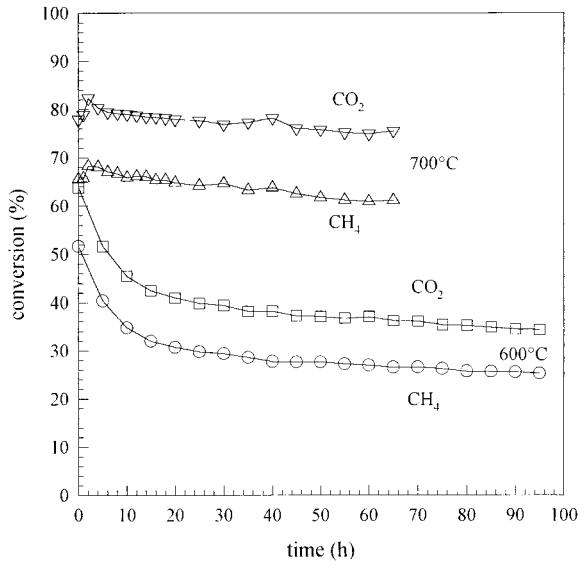

FIG. 3. Deactivation as a function of time at different temperatures for calcined samples.

mixture re-admitted. This cycle was repeated 12 times with varying time intervals, up to a total time-on-stream of about 80 h. Figure 2 shows the methane conversion, the average particle size and the degree of ferromagnetic nickel as a function of time-on-stream.

As observed previously, the catalyst immediately showed a high activity. Some fluctuations in the conversion at the beginning of the run might be caused by the quenching/heating procedure. The overall deactivation of the catalyst over the run was 0.1% h^{-1}, in line with the aging rate reported in Table 1. After 5 min of reaction the percentage of ferromagnetic nickel (equal to zero before the catalytic run) already reached more than 47%. This percentage strongly increased up to a nearly constant level of 90–95% after 3 h on stream. At the same time the mean particle size increased slowly and continuously, attesting some regular sintering process of the nickel phase. The size distribution remained narrow, without the formation of particles larger than 150 Å (no remanent magnetization).

Influence of the reaction temperature on catalyst deactivation. The temperature dependence of the deactivation process was investigated by way of stability tests carried out at 600 and 700°C. Figure 3 shows the conversion of methane and of carbon dioxide at 600 and 700°C as a function of time for two samples that were only precalcined. It can be seen that the initial nonlinear deactivation was much more important at 600°C than at 700°C. The subsequent linear deactivations were comparable. The same marked temperature dependence in the ageing profile was also observed for samples prereduced at 750°C (Fig. 4). Similar nonlinear profiles were obtained at 600°C for both precalcined and prereduced samples, though the prereduced catalyst presented a lower activity than the precalcined catalyst.

The final degree of ferromagnetic nickel and of dispersion was 77 and 17%, respectively, after a test at 600°C for 90 h on a prereduced sample. Thus, as at 700°C, a significant lack of ferromagnetic nickel was still observed at 600°C for a prereduced sample. Almost no particle sintering occurred at 600°C, in contrast to the observation at 700°C (Table 1).

TPH study of carbon deposits. In order to characterize the carbon deposited on the catalyst during the reforming

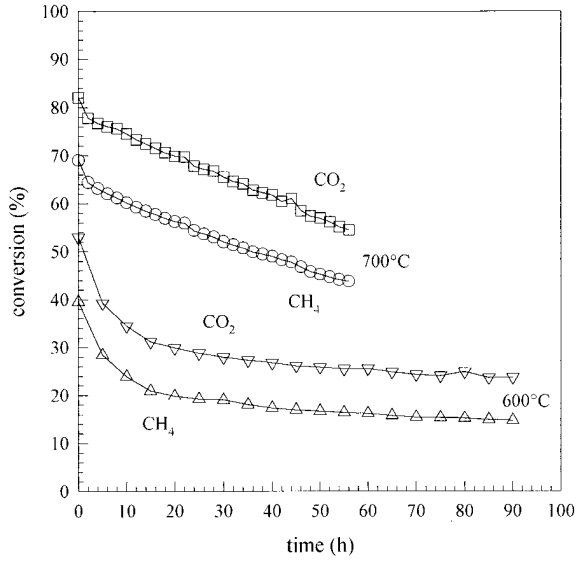

FIG. 4. Deactivation as a function of time at different temperatures for reduced samples.

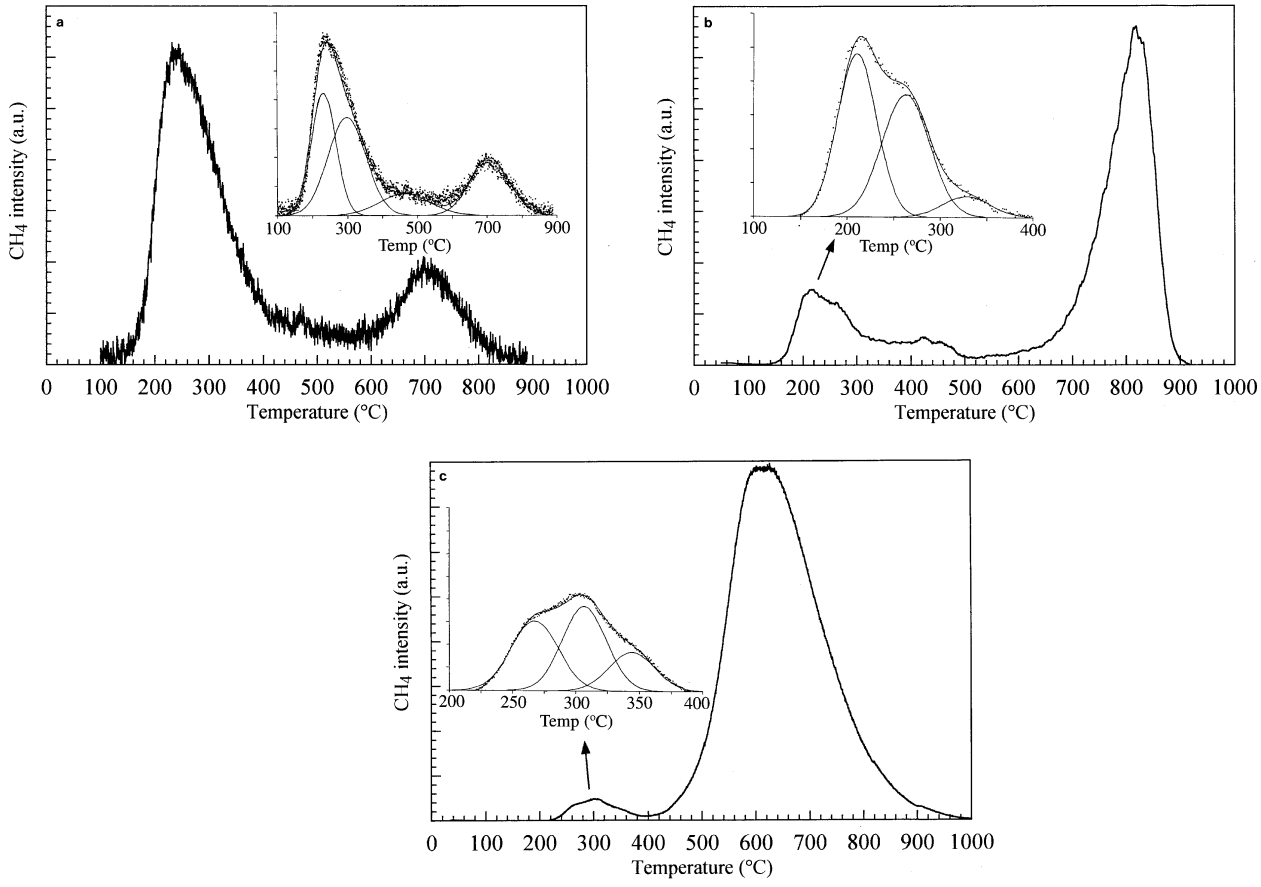

FIG. 5. (a) Result of TPH experiment after 10 min time-on-stream. (b) Result of TPH experiment after 1 h time-on-stream. (c) Result of TPH experiment after 67 h time-on-stream.

reaction, TPH experiments were carried out after reaction at 700°C on a precalcined and nonreduced sample.

The results of the TPH experiments carried out after 10 min, 1 h, and 67 h on stream are shown in Figs. 5a, 5b and 5c, respectively. Several narrow or broad peaks of methane (and ethane for some of them) corresponding to various forms of carbon deposits were observed with relative intensity changing drastically with time-on-stream. When there was evidence of several combined peaks under a broad one a deconvolution procedure was undertaken.

After 10 min of reaction (Fig. 5a) only methane was detected. The main peak was observed at low temperature (between 120 and 300°C), which could be decomposed into two peaks at 230 and 300°C. Smaller peaks developed at higher temperature (460 and 710°C).

After 1 h of reaction (Fig. 5b) methane was still the only product from carbon hydrogenation. Nearly the same low and medium temperature peaks were observed below 500°C. In contrast, a much larger peak developed at around 820°C.

After 67 h on stream (Fig. 5c) TPH peaks corresponding again to two distinct ranges of temperature were observed, as follows:

(i) The first group of methane peaks between 200 and 400°C was decomposed into three separate peaks, in a similar way as for the previous TPH diagrams. The first peak of methane with a maximum at around 270°C was actually exactly superimposed by a peak of ethane of close intensity ($C_{CH_4}/C_{C_2H_6} = 1.4$). The second and third peaks at 310 and 340°C, respectively, were formed essentially of methane and were rather similar to the corresponding peaks already detected for shorter time-on-stream.

(ii) The high temperature peaks actually appeared as a large and broad peak between 400 and 900°C with a maximum at around 650°C, most probably including the different types of high temperature peaks observed separately in the previous cases.

The precise amounts of carbon corresponding to each identified peak were calculated from the peak areas and expressed in terms of the C/Ni_s^0 atomic ratio, where Ni_s^0 represents the number of surface nickel metal atoms determined from magnetic measurements carried out after times-on-stream corresponding to the three reported TPH experiments. These data are reported in Table 2. As can be seen, the first low temperature peak ($T < 270$°C) corresponded to nearly constant values of the C/Ni_s^0 ratio, between 0.33 and

TABLE 2

Amounts of Carbon Measured from the Deconvoluted TPH Peaks, Expressed in Term of the Atomic Ratio C/Ni_s^0, the Number of Surface Nickel Atom Ni_s^0 Being Determined from the Magnetic Measurements Carried out after the Corresponding TPH Experiments

Time on stream at 700°C	Atomic C/Ni_s^0 (peak maximum temperature (°C))					Total C/Ni_s^0
10 min	0.36 (230)	0.45 (300)	—	0.13 (460)	0.27 (710)	1.21
1 h	0.33 (240)	0.30 (290)	0.05 (330)	0.21 (425)	2.74 (820)	3.63
67 h	0.39[a] (270)	0.26 (310)	0.12 (345)	22.4 (400–900)		23.17

Note. The temperatures corresponding to the peak maxima or the temperature range for broad peaks are reported in parentheses.

[a] Sum of 0.23 from methane and 0.16 from ethane formation.

0.39. The second low temperature peak (at around 300°C) presented similar C/Ni_s^0 values, though slightly decreasing with time on stream.

Besides the low temperature carbon species, more stable carbon species, hydrogenated at intermediate (around 300–340°C) and higher (between 400 and 900°C) temperature were accumulating as a function of time on stream (Table 2). Thus, after 67 h on stream, the hydrogenation of the large high temperature peak represented around 60 and 10 times the amount of high temperature carbon observed after 10 min and 1 h on stream, respectively.

In order to follow the changes in the magnetic state of the Ni particles as a function of carbon deposition, a TPH experiment was carried out in the magnetic cell after a 4 h aging run and interrupted at 325°C, i.e., after the hydrogenation of the most reactive carbonaceous species. The content of ferromagnetic nickel was 90% after the aging run. This content reached 100% after the first step of the TPH (from room temperature to 325°C). The TPH was then continued up to 800°C and the ferromagnetic signal remained constant. No water was detected during the experiment, which discarded the presence of NiO which would have been reduced under hydrogen flow. The above experiment demonstrated that the highly reactive carbonaceous species corresponding to the two low temperature TPH peaks were in chemical interaction with the nickel metal phase, i.e., able to withdraw the related Ni atoms from the collective ferromagnetism of the particle. As an example, the formation of carbide-like species which implies the formation of Ni–C bonds is known to decrease the ferromagnetic signal of Ni particles (14). Inferentially, the absence of change in the ferromagnetic signal during the further medium and high temperature TPH step indicated that the corresponding carbon deposits were accumulating outside the Ni particles, as will be confirmed by TEM, without chemical bonding with the nickel phase (either outer surface or on the silica support).

In order to check the effect of pretreatment conditions on coke deposition, the above results obtained with a precalcined sample can be compared to the already reported data obtained by TPO under similar aging conditions with a prereduced sample (9). Note that for similar catalyst treatment and aging conditions, no significant difference was observed in the total amount of carbon deposits between TPO and TPH techniques. Differences were observed only for the temperature of peak maxima as expected by comparing the combustion reaction for TPO with the hydrogenation reaction for TPH. After 2 and 20 h on stream, the C/Ni_s^0 ratios obtained with a prereduced sample were 0.64 and 15.8, respectively, which tended to indicate that slightly lower accumulation of coke occurred on prereduced samples than on precalcined ones.

TEM study of particle morphology and carbon deposits. Samples corresponding to the various conditions of pretreatment (i.e., calcination or reduction) and of reaction described above were prepared in the microreactor for TEM investigation.

After calcination at 750°C (Fig. 6a) the fresh catalyst presented a layered bidimensional phase (7–14 nm length and 0.5–1.0 nm thickness) deposited on the silica support, characteristic for nickel hydroxide or hydrosilicate. Note that the hydroxide structure is unlikely to remain stable during the high temperature treatment of the catalyst. Therefore the TEM observation of the layered structure could indicate the presence of hydrosilicate compounds (more stable under the prevailing conditions) or be due to a possible rehydroxylation of the samples during the procedure applied for TEM analysis.

After 10 min on reforming stream at 700°C, this layered structure almost vanished and fuzzy particles were observed with a diameter ranging between 3.5 and 5.0 nm.

After 3 h on stream at 700°C (Fig. 6b) more contrasted particles were observed, which most probably corresponded to the almost completely reduced state as revealed by magnetic measurements. The size distribution, however, was somewhat heterogeneous. Large as well as relatively small particles were observed. A number of particles tended to be flat polyhedrals presenting a typical size of 6–7 nm length and 4 nm width. Several crystallographic

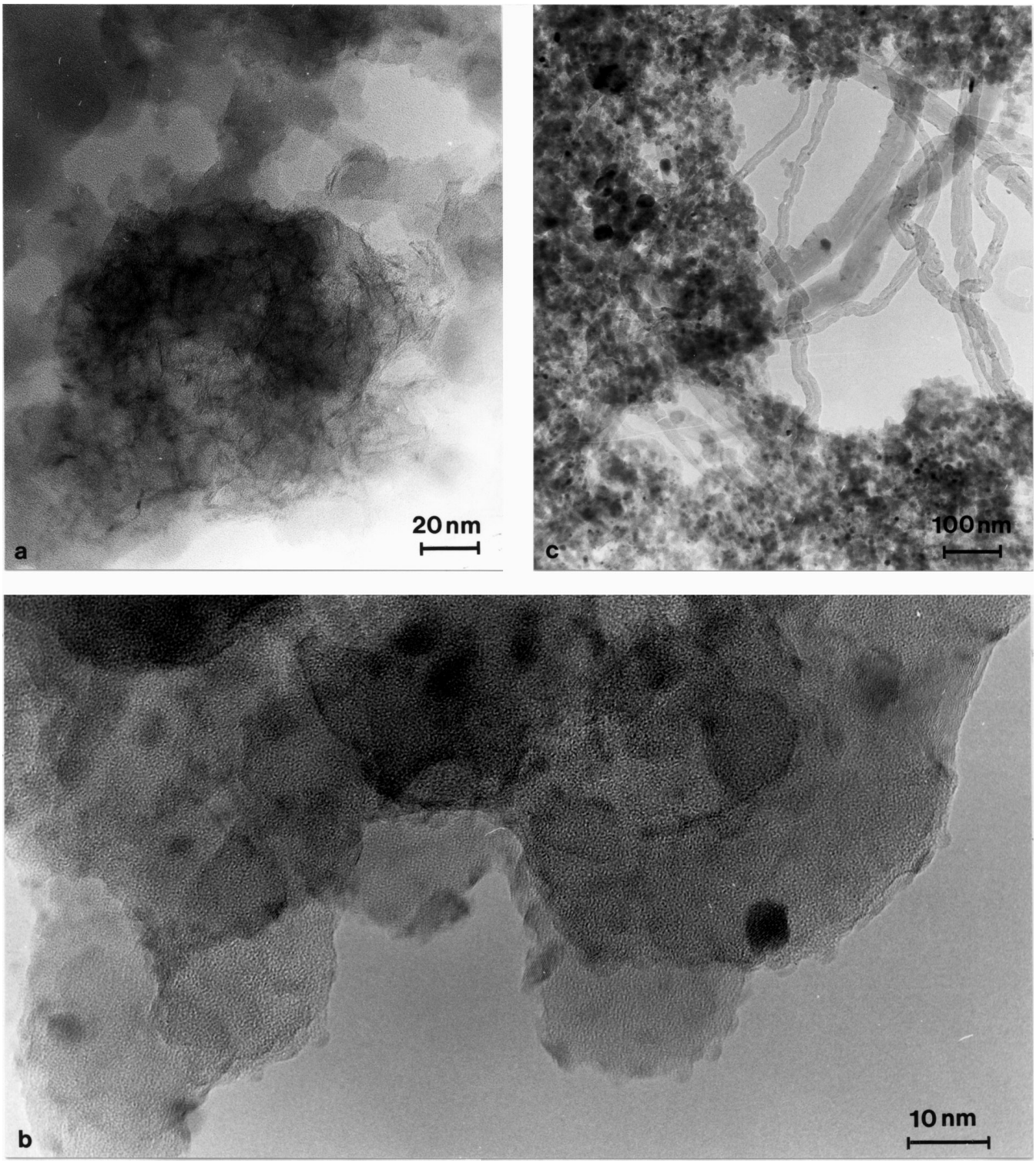

FIG. 6. TEM picture of (a) a calcined sample before reaction, (b) a calcined sample after 3 h on stream, and (c) a calcined sample after 67 h on stream.

orientations were measured, among them the ⟨111⟩ planes characteristic for cubic nickel in the metallic state. No forms of carbon were visible.

After 67 h on stream at 700°C (Fig. 6c) the particle size distribution was still heterogeneous and most of the particles were stuck on the silica support. A few hollow carbon filaments were observed. Most of them were irregular and were constituted of graphitic carbon (as deduced from a measured interreticular distance of 3.34 Å). The internal diameter of the filaments corresponded generally to the diameter of the particle located on top or inserted within the filament. However, the thickness of the carbon wall varied. Their shape suggested that they resulted from noncontinuous growing processes, as generally observed for this kind of carbon whisker (12, 13).

After 56 h of reaction at 600°C carried out on a precalcined sample, graphitic filaments were observed, although less than at 700°C. However, the total amount of carbon was larger. Layered nickel hydroxide or hydrosilicate structures were still observed on the support.

After reduction at 750°C (Fig. 7a) the fresh catalyst presented well dispersed spherical particles, with a diameter ranging between 4.0 and 6.0 nm, which corresponded to the mean size determined by magnetic measurements (6.3 nm in Table 1). After 3 h of reaction this structure was still observed, and the nickel particles remained relatively small and homogeneously distributed. In addition, an amorphous form of carbon veils and ribbons tended to develop around the particles. Large amounts of these bidimensional forms of carbon as well as some carbon filaments were observed after 65 h of reaction (Fig. 7b). The nickel particles stayed small and homogeneously dispersed.

TGA study of carbon deposits. Figure 8 shows the results of the TGA experiments as a function of pretreatment and reaction temperature. It can be seen that all the coking profiles presented similar trends namely: (i) an induction period (visible even on curve d after rescaling the *y*-axis), (ii) an acceleration of the coking rate, and (iii) a decrease of the coking rate. The total amount of deposited coke tended to level off for a sufficiently long run period. However, despite these common features the coking patterns were highly dependent on pretreatment conditions and aging temperature. At a given temperature the reduced samples exhibited a lower tendency toward coking than the samples that were not reduced. Thus, at 700°C the amount of coke deposited on a reduced sample after 25 h on stream was very low (3 mg_{coke}/g_{cat} in Table 3) and approximated the lower measuring limit of the balance. The amount of coke deposited at 700°C corresponding to the calcined and nonprereduced sample was around 100 times higher. For given pretreatment conditions the amount of deposited coke was much higher at 600°C than at 700°C (two orders of magnitude greater than for reduced catalysts). If one now compares the amounts of coke determined by TGA and by TPH/TPO (Table 3) a reasonable agreement is obtained for reduced samples run at 700°C (3 vs 16 mg_{coke}/g_{cat}), i.e., for the case of poorly active catalysts for coke deposition. However, a large discrepancy is noted for calcined samples (300 vs 25 mg_{coke}/g_{cat}), i.e., for the case of highly active catalysts for coke deposition.

TABLE 3

Amount of Coke Deposits Measured by TGA and by TPH/TPO

Pretreatment	Reaction temperature (°C)	Time on stream (h)	Total amount of coke (mg_{coke}/g_{cat})	
			TGA	TPH/TPO
Calcined	700	67	300	25
	600	4	507	—
Reduced	700	20	3	16
	600	20	374	—

Although it was not possible to measure the catalytic activity during TGA experiments, a likely hypothesis is that the observation of nearly constant amounts of carbon after certain times on stream (3 to 15 h, curve d after rescaling, and c and b, respectively) was simply due to an almost complete deactivation of the catalysts in the microbalance. When the reaction was carried out in a microreactor under equivalent experimental conditions the catalyst samples still showed a reasonable activity at similar time-on-stream. To explain the discrepancy between the two systems for the case of active catalysts, it can be noted that the gravimetric system was equipped with a perforated basket instead of a plug flow fixed bed reactor as used for aging/TPH/TPO experiments. Thus, much higher temperature gradients throughout the catalyst bed in the microbalance, induced by the endothermicity of the reaction, might have encouraged the Boudouard coking reaction, which is thermodynamically favored at low temperature (15). We will therefore consider that the final state of the TGA system corresponded to complete catalyst deactivation, in contrast with the TPH or TPO experiments carried out on still active samples. The sensitivity toward pretreatment parameters and reaction temperature are, however, assumed to be comparable for both systems.

DISCUSSION

Several complex phenomena such as nickel phase sintering, changes in the degree of ferromagnetic nickel and carbon deposition were observed during catalytic runs carried out on Ni/SiO_2 catalysts under CO_2 reforming conditions, at either 600 or 700°C. Key parameters such as pretreatment conditions, reaction temperature, and the initial state of the nickel phase were shown to determine to a large extent the aging rates of the tested catalysts. A prerequisite for

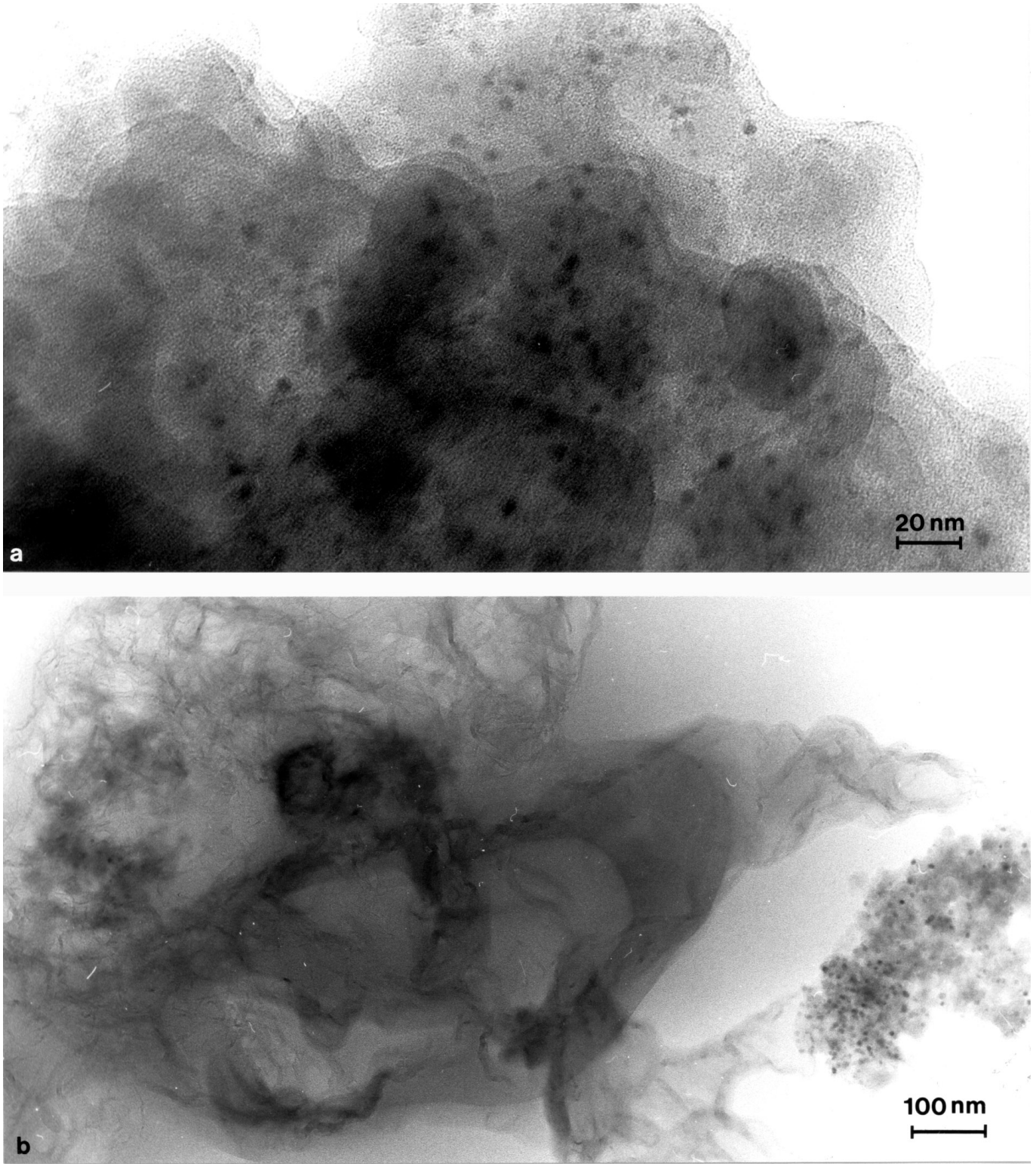

FIG. 7. TEM pictures of (a) a reduced sample before reaction and (b) a reduced sample after 65 h on stream.

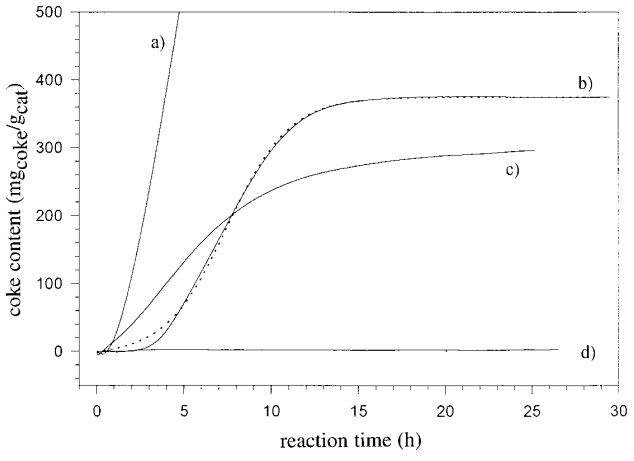

FIG. 8. Results of TGA experiments at different reaction temperatures and different pretreatments. Solid lines, experimental data. (a) Unpretreated and tested at 600°C, (b) reduced and tested at 600°C, (c) calcined and tested at 700°C, (d) calcined, reduced, and tested at 700°C. Dotted line, modeling of experiment at 600°C using a reduced sample.

understanding these aging phenomena is indeed to identify the actual nature of the active phase at each step of the catalytic run.

Nature of the active phase. Several features can be considered for describing the active phase of a Ni/SiO_2 catalyst under CO_2 reforming conditions:

(i) Initial activities (methane and carbon dioxide conversion measured after 5 min on steam, corrected for the Ni dispersion in the case of badly dispersed samples) were found to be very close for all the tested catalysts, irrespective of their pretreatment (untreated, calcined, or reduced). This suggests that as soon as contact is made with the reacting mixture, a common active phase is developed at the catalyst surface.

(ii) For the case of nonpretreated or simply calcined samples, the magnetic measurements indicated that after 5 min on stream, more than 45% of the Ni phase was already ferromagnetic, i.e., under the metallic state, pointing out the strong reductive character of the reaction mixture. After 3 h the content of ferromagnetic nickel reached a nearly constant level of 90–96%. If one compares the change in conversion with the degree of ferromagnetic nickel and accounts for the slight sintering which occurred at the same time, it is observed that although the amount of metallic nickel doubled, the activity of the catalyst decreased slightly (Fig. 2). This indicates that the active phase of nickel was not the metallic nickel but another phase, which was formed immediately after contacting the initial oxide phase with the reacting mixture.

(iii) TPH experiments clearly indicated that highly active forms of carbon built up in the very initial period of the catalytic run, remaining stable all over the run. In addition, these carbon deposits were found to be chemically bound to metallic nickel. They were actually formed of at least two distinct species:

— The most reactive one led to an atomic ratio $C/Ni_s^0 =$ 0.33–0.39 (Table 2). As no evidence of surface C–H bonds was provided by *in situ* DRIFTS experiments carried out after some minutes on stream (see Part II of this study (16)), it was assumed that these carbonaceous species were completely dehydrogenated, which would account for their high reactivity toward hydrogen. Within this assumption, the above ratios correspond to the stoichiometry of nickel carbide between Ni_3C and Ni_2C. Independent measurements of the reactive intermediate accumulation under steady-state conditions by isotopic transient kinetics (see Part II of this study) led to a consistent value of $C/Ni_s^0 = 0.53$. Besides methane, ethane was also detected during the hydrogenation of the most reactive carbon deposits after long time-on-stream. This suggests that some dimer C–C species formed progressively on the surface in addition to the monomer carbide-like species. This progressive carbon organization would account for the slight shift to higher temperature observed for the peak maximum (230–240 to 270°C in Table 2). Though concerning polycrystalline structures, these proposals of surface carbide-like species are in good agreement with fundamental studies carried out on single crystals indicating that Ni(100) and Ni(111) surfaces could accommodate atomic carbon up to a $1:2$ $C:Ni_s^0$ atomic ratio (17, 18).

— The slightly less reactive carbon species (hydrogenated at 300–310°C), also bound to nickel atoms, corresponded to similar C/Ni_s^0 values (0.45 to 0.26 in Table 2). This species can reasonably be assigned to the formation of a nickel carbide sublayer or interstitial carbon. No ethane was detected during the hydrogenation of these species as expected for the hydrogenation of bulk atomic carbon species. Within this assumption, the slight decrease in the C/Ni_s^0 ratio which occurred with time on stream could correspond to the shift from Ni_2C to Ni_3C, in line with the migration of C atoms through the nickel particles and/or the morphological changes observed by TEM as discussed below.

Nickel carbide and interstitial carbon are known to decrease the ferromagnetism of a Ni particle: the former does so by impeding 2 or 3 atoms from participating in the collective ferromagnetism, the latter by decreasing the saturation magnetization owing to the screening in the nickel d-band of the 4 electrons of the C atom (14). Accounting for a nickel dispersion of 14% on aged samples (Table 1), the above proposal of carbide-like monolayer formation and interstitial dissolution of one monolayer equivalent should lead to a decrease of the nickel ferromagnetism of around 20–25%. Thus the final content of ferromagnetic nickel should have been 75–80%, a value slightly lower than the 90–96% reported above. This difference could come from some carbon diffusion outside the particles and oxidation

when the reactor was flushed with He at 700°C before the magnetic measurements. As a matter of fact, interstitial carbons are known to be rather unstable and easily migrating outside the particles (14). Furthermore, as reported in Part II of the study, when switching from the reacting mixture to pure He (as is done for carrying out the magnetic measurements), there was observed some residual CO formation which could correspond to a partial oxidation of surface carbon by traces of oxygen present in the helium flux.

From the above observations, it is therefore proposed that the actual active phase for the carbon dioxide reforming of methane is a nickel carbide-like layer, formed at the particle surface as soon as it is contacted with the reacting mixture, whatever the initial state of the catalyst. The proper mechanism of the reforming reaction involving this active phase will be detailed in Part II of the study (16). Some carbon, equivalent to a carbide sublayer also dissolves rapidly. This evidence of carbon diffusion through the particles could be related to the formation of external carbon deposits, as will be discussed later. Note that although carbon monomer species are often postulated as reacting intermediates in CO_2 reforming reaction (3, 19), no clear quantification and proposal of the actual state of the active surface of nickel catalysts was proposed up to now to our knowledge. This state of the surface under reforming conditions could be specific to the nickel phase. For Rh/SiO_2 catalysts Mark and Maier (20) recently observed that the catalyst could accommodate more than 15 monolayers of carbon and still be able to dissociate methane. These authors admitted, however, that under the proper reforming conditions, i.e., cofeeding methane and carbon dioxide, the rapid reaction of the active carbon with CO_2 could avoid a high surface coverage of carbon. The interesting and converging point between the latter work and our study is that the actual active phase for reforming is not the metal itself but a carbided form of the metal, or even surface carbon atoms which could be considered as active centers by themselves.

If one now considers that the active surface carbide phase builds up in the very beginning of the catalytic run, the question remains to understand how morphological and structural changes in the Ni particles, and also the development of other forms of toxic carbons may affect the catalytic behavior of the active phase and lead to the observed deactivation phenomena.

Ni particle changes with time-on-stream. As already stressed, two different cases have to be considered, depending on the activation conditions.

For nonprereduced samples, the TEM analysis clearly showed that the initial layered structure, characteristic for $Ni(OH)_2$, was rapidly transformed into particles presenting various sizes with a marked trend to form flat polyhedrals with a typical size of 6–7 nm length and 4 nm width. Although some particles were found to be extracted from the silica surface by carbon filaments (nickel particles observed on top or inside the filaments), most of the particles appeared to be stuck to the silica surface, even after a long period on stream. The formation of a thin interface layer of nickel hydroxy-silicate such as $Ni_3[SiO_5](OH)_4$ could be proposed to explain the topotactic growth of the nickel particles during the reduction under reaction conditions. As a matter of fact, such a silicate interface was shown to form on Ni/SiO_2 catalysts preferentially in the presence of water. Even at low partial pressures, as during a fast reduction, it acts as a glue favoring the thermal stability of nickel particles (21, 22).

For prereduced samples, at variance with the above case, the well dispersed spherical particles formed during the reduction procedure did not undergo major morphological changes during the catalytic run, except some increase in the mean particle diameter (from 63 to 78 Å in Table 1). It can also be noted that for these samples the content of ferromagnetic nickel was rather low after reduction at 750°C (62%) and slightly increased during the catalytic run (up to 71%). The apparently uncompleted reduction can actually be assigned to the formation of a bulk Ni–Si alloy which was assumed elsewhere to develop during reduction under similar conditions (23). As a matter of fact, with only 11.5 at.% of silicon in nickel metal, which corresponded to the limit of Si solubility, the Ni–Si alloy was no more ferromagnetic at room temperature. It may therefore be deduced from the ferromagnetic signal obtained for our sample that about 7% of silicon was alloyed with nickel. No evidence of Ni–Si alloy was, however, obtained from EDX analysis carried out during the TEM study possibly due to some amorphous character of this alloy and due to the fact that the Ni signal was always superimposed on the very large silica signal. Fortunately, this alloy, which was not observed for the sample reduced under severe conditions at 900°C (Table 1), has never been reported as inducting special properties for the Ni particles. Moreover, it is likely to progressively demix under the redox catalytic cycles, which would account for the increase in the ferromagnetic signal.

To summarize, although a similar active phase rapidly built up on the surface, quite different morphological evolution of the nickel phase during the catalytic runs was observed depending on the pretreatment procedure. Figures 9a and b tentatively illustrate these two types of nickel phase evolution.

Some comments can be added concerning the sintering processes which could be involved during these morphological changes. No loss of nickel was observed after long-term runs, whatever the pretreatment. Moreover, no very small particles appeared with time on stream. A sintering process by atomic species migration of "Ostwald ripening" (24, 25) can therefore be discarded. Indeed, such a mechanism which implies nickel vaporization would proceed at much higher temperature. In contrast, the observed trend

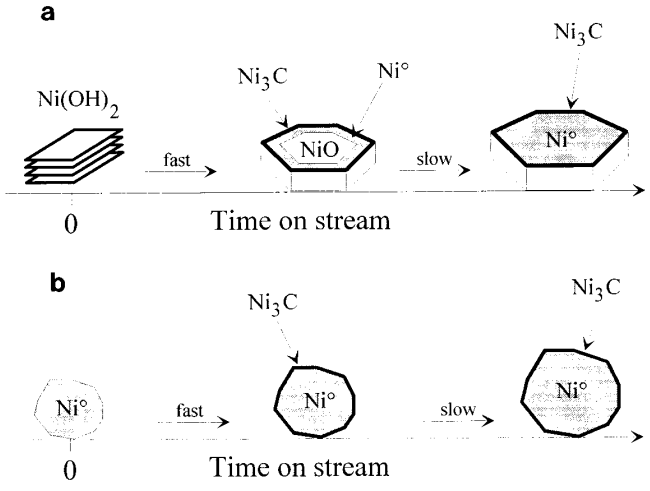

FIG. 9. Simplified model of the changes during reaction of (a) a calcined catalyst sample and (b) a reduced catalyst sample.

for small particles to disappear together with the appearance of larger particles (maintaining a monomodal size distribution) corresponded well to a sintering process via particle migration and coalescence (26). Such a nickel transport process is quite plausible at 600–700°C, i.e., slightly above the Tammann temperature of nickel (600°C).

The question now arises as to how far the loss of active surface by the sintering effect can account for the observed deactivation rates.

— For the case of a non-pretreated sample (Fig. 2), the loss of active surface over 75 h on stream amounted to around 13%, taking into account the progressive reduction of nickel and the particle model depicted in Fig. 9a. Meanwhile, the conversion at 700°C decreased by 11% (Table 1). Taking into account the model uncertainties, it can be concluded that the deactivation observed with nonprereduced catalysts was satisfactorily accounted for by the simple loss of active surface due to nickel sintering. Note that much lower aging rates were obtained in a microreactor, by avoiding the numerous quenching/heating cycles used in the above magnetic cell experiment (Table 1, last line).

— For the case of a prereduced sample, the deactivation at 700°C (Fig. 1c, Table 1) amounted to 36% within 65 h on stream while the nickel dispersion decreased by 18% (Table 1). This result clearly indicates that besides the loss of active surface by nickel sintering, another factor such as deposition of toxic carbon has to be considered for explaining the catalyst aging.

Carbon deposits with time on stream. TPH studies have demonstrated that besides the initial fast formation of reactive carbon on and within the nickel particles, other more stable forms of carbon were slowly accumulating with time on reforming stream. From TEM studies, the latter forms appeared to depend on the pretreatment conditions as well as the reaction temperature.

— For nonprereduced samples, only a few carbon filaments were observed after several hours on stream at 700°C. Since this catalyst deactivated mostly due to sintering as shown above, it can be deduced that this form of filamenteous carbon is not toxic toward the reforming reaction under the chosen operating conditions (700°C). Thus, under TGA conditions where temperature gradients are expected to occur 10 times more carbon (Table 3) than under TPH conditions led to an effective decrease in the rate of carbon deposition.

— For prereduced samples, both filamenteous and proteiform (veils and ribbons) carbons were detected under similar conditions. Assuming the nontoxicity of filaments, it can be deduced that the part of the observed deactivation not related to sintering was due to the proteiform deposits. These bidimensional structures (Fig. 7b) would act as encapsulating carbon, most likely hindering the diffusion of reactants to the active surface. Their high toxicity was proved under TGA conditions where very low amounts of deposits were shown to stop any further carbon deposition, strongly suggesting that the catalyst was rapidly killed by these deposits. A modeling of the TGA curves, to be detailed in Ref. (27), was undertaken on the basis of a classical model assuming two types of coke formation (28). One type of coke C_1 deposited as a function of the remaining bare surface (surface poisoning) and another type C_2 deposited both as a function of the remaining bare surface and of the already deposited code (chain growth),

$$dC_1 = k_1 \cdot (S - C) \cdot R \cdot V \cdot dt \quad [1]$$

$$dC_2 = k_2 \cdot (S - C) \cdot C \cdot R \cdot V \cdot dt \quad [2]$$

$$C = C_1 + C_2, \quad [3]$$

where k_1 and k_2 are rate constants, R the concentration of reactants, V the total flow rate, S the total active surface, and C the total percentage of coke deposited.

A reasonable fit was obtained as depicted in Fig. 8, confirming our hypothesis of progressive poisoning of the catalysts under TGA conditions. Further improvement of the model assuming the poisoning of several sites together by coke deposition and also further TGA experiments under more controlled operating conditions are in progress.

Whatever the pretreatment, it was also shown that at lower temperature ($T = 600$°C), faster deactivation occurred, essentially due to carbon deposits since the thermal sintering effect was markedly decreasing, if not vanishing. TEM analyses clearly indicated the accumulation of proteiform carbon at low temperature, thus reinforcing the above conclusions about its toxicity.

Structure sensitivity of coke deposition. As already stressed, the carbide-like surface deposits forming the

active phase were shown to be structure insensitive since they were found to be independent of the state of reduction and of the size of nickel particles.

Numerous works have already been devoted to the mechanism of filamenteous carbon growth, essentially under steam reforming conditions (12, 13, 29). Without going into details, the formation of hollow filaments enclosing faceted particles and the evidence of interstitially dissolved carbon strongly suggest similar processes under CO_2 reforming conditions, i.e., carbon migration through the particle and excretion as graphite layers on suitable crystallographic surfaces, most probably ⟨111⟩ planes according to Boellaard *et al.* (29). This type of dense plane was clearly identified on nonprereduced samples by microdiffraction analysis on TEM pictures. Thus the morphological trend to develop faceted and flat particles for samples reduced under the reaction conditions would possibly favor the carbon migration and excretion along given planes and in a given direction, without particle encapsulation and deactivation. Moreover, the topotactic growth of particles and the likely silicate interface formation would keep most of the particles stuck on the silica surface. This would explain why the nonprereduced samples may exhibit a very stable activity at 700°C for a long period, though accumulating nontoxic coke. At lower temperature, or under TGA conditions where temperature gradients probably occur, a faster deactivation results from a considerable acceleration of coke deposition.

For the case of prereduced samples, no specific crystallographic plane orientation was observed, whatever the initial particle size distribution. This means that the particle surface can be considered as a complex combination of microfacets presenting a high concentration of edges, corners, and various types of surface defects, without developing an interface with the silica surface (see Fig. 9b). According to this, the carbon growth is expected to proceed in all directions around the particle, rapidly forming a diffusion barrier for reactants and products and leading to the progressive isolation of the active surface from the reacting mixture.

CONCLUSION

The deactivation of Ni/SiO_2 catalysts under CO_2 reforming conditions was shown to result from numerous but interconnected parameters. Initially, and whatever the pretreatment, a carbide-like surface forms rapidly, presenting a catalytic activity little dependent on the particle morphology and the degree of nickel reduction. During time-on-stream, slight particle sintering occurs (most likely through a particle migration and coalescence process) and various forms of coke accumulate outside the particles. In contrast with the reforming activity, the coke formation (rate and type) appears to be highly structure sensitive, which markedly determines the aging of the working material:

— Faceted and flat particles obtained from a reduction under the reaction conditions tend to produce essentially no or little toxic filamentary carbon.

— Small and spherical particles obtained from a prereduction under hydrogen tend to produce highly toxic encapsulating carbon.

— At temperature lower than 700°C, less particle sintering but considerably higher rates of coke deposition are observed in agreement with thermodynamic considerations. In this case the deactivation rate tends to be independent of the particle treatment and morphology.

The optimized conditions for catalyst stability were obtained without prereducing the catalyst, at an operating temperature of 700°C and in a reactor where temperature gradients were minimized.

ACKNOWLEDGMENTS

This work has been supported by the EEC Joule II Programme. Dr. C. Leclercq is acknowledged for providing and discussing the TEM micrographs. Prof. A. Monzon and Dr. J. C. Rodriguez from the University of Zaragoza (Spain) are acknowledged for performing the TGA experiments.

REFERENCES

1. Fox, J. M., *Catal. Rev.-Sci. Eng.* **35**, 169 (1993).
2. Gadalla, A. M., and Bower, B., *Chem. Eng. Sci.* **43**, 3049 (1988).
3. Rostrup-Nielsen, J. R., and Bak Hansen, J.-H., *J.Catal.* **144**, 38 (1993).
4. Richardson, J. T., and Paripatyadar, S. A., *Appl. Catal.* **61**, 293 (1990).
5. Tsang, S. C., Claridge, J. B., and Green, M. L. H., *Catal. Today* **23**, 3 (1995).
6. Sacco, A., Geurts, F. W. A. H., Jablonski, G. A., Lee, S., and Gataly, R. A., *J. Catal.* **119**, 322 (1989).
7. Jablonski, G. A., Geurts, G. W. A. H., Sacco, A., and Birdemann, R. R., *Carbon* **30**, 87 (1992).
8. Nolan, P. E., Lynch, D. C., and Cutler, A. H., *Carbon* **32**, 477 (1994).
9. Swaan, H. M., Kroll, V. C. H., Martin, G. A., and Mirodatos, C., *Catal. Today* **21**, 571 (1994).
10. Martin, G. A., Mirodatos, C., and Praliaud, H., *Appl. Catal.* **1**, 367 (1981).
11. Selwood, P. W., "Chemisorption and Magnetisation." Academic Press, New York, 1975.
12. Rostrup-Nielsen, J. R., *in* "Catalysis, Science and Technology" (J. R. Anderson and M. Boudart, Eds.), Vol. 5, p. 1. Springer-Verlag, Berlin, 1984.
13. Bartholomew, C. H., *Catal. Rev.-Sci. Eng.* **24**, 67 (1982).
14. Mirodatos, C., Dalmon, J. A., and Martin, G. A., *in* "Catalysis on the Energy Scene" (S. Kaliaguine and A. Mahay, Eds.), p. 505. Elsevier, Amsterdam, 1984.
15. de Bokx, P. K., Kock, A. J. H. M., Boellaard, E., Klop, W., and Geus, J. W., *J. Catal.* **96**, 454 (1985).
16. Kroll, V. C. H., Swaan, H. M., Lacombe, S., and Mirodatos, C., *J. Catal.*
17. Gauthier, Y., Baudoing-Savois, R., Heinz, K., and Landskron, H., *Surf. Sci.* **251/252**, 493 (1991).
18. Kilcoyne, A. L. D., Woodruff, D. P., Robinson, A. W., Lindner, Th., Somers, J. S., and Bradshaw, A. M., *Surf. Sci.* **253**, 107 (1991).

19. Solymosi, F., Kutsán, G., and Erdöhelyi, A., *Catal. Lett.* **11**, 149 (1991).
20. Mark, M. F., and Maier, W. F., *Angew. Chem. Int. Ed. Engl.* **33**, 1657 (1994).
21. Geus, J. W., *in* "Scientific Bases for the Preparation of Heterogeneous Catalysts" (G. Poncelet *et al.*, Eds.), p. 1. Elsevier, Amsterdam, 1983.
22. Mirodatos, C., Dalmon, J. A., Garbowski, E. D., and Barthomeuf, D., *Zeolites* **2**, 125 (1982).
23. Praliaud, H., and Martin, G. A., *J. Catal.* **72**, 394 (1981).
24. Wynblatt, P., and Gjostein, N. A., *Prog. Solid State Chem.* **9**, 1 (1975).
25. Flynn, P. C., and Wanke, S. E., *J.Catal.* **37**, 432 (1975).
26. Ruckenstein, E., and Pulvermacher, B., *J. Catal.* **29**, 224 (1973).
27. Kroll, V. C. H., Monzon, A., Rodriguez, J. C., and Mirodatos, C., in preparation.
28. Dadyburjor, D. B., and Liu, Z., *Chem. Eng. Sci.* **47**, 645 (1992).
29. Boellaard, E., de Bokx, P. K., Kock, A. J. H. M., and Geus, J. W., *J. Catal.* **96**, 481 (1986).